

Measurement of the Heat Transfer Coefficient in Case of Impinging Synthetic Jet

Petra Dancova, Tomas Vit, and Jan Novosad

Technical University of Liberec, Czech Republic

Abstract: The paper deals with the measurement of a heat transfer coefficient caused by an impinging synthetic jet. The heat transfer coefficient is measured using the thermoanemometry in a constant temperature mode (CTA). Experiments are based on measurement and evaluation of heat flux from the heated probe (placed on the heated plate) to the surrounding fluid. The probe temperature is maintained similar to the temperature of the plate to minimize the conductive heat flux from the probe to the plate. Experiments are performed with three different overheat ratios of the thermoanemometric probe.

The experimental results are the starting point for the CFD simulations. CFD simulations are carried out in a pimpleFoam solver included in a OpenFOAM software modified by adding an energy transport equation. The simplified computational domain is defined based on the experimental setup. CFD boundary conditions are set according to the experimental data. CFD results are velocity fields in the whole computational domain. Velocity fields are confronted with experimental data to validate the developed OpenFOAM solver which will be used for next numerical investigation of heat transfer.

Key words: synthetic jet, heat transfer, thermoanemometry, OpenFOAM

1. Introduction

Subject of heat transfer intensification is heavily solved today. The topic is of great importance especially in the field of cooling of micro-electronics devices. Each electronic device generates heat that grows proportionally with the number of elements in the circuit. This heat has to be removed from the device in order to ensure its functionality within the technically permissible operating temperature and to avoid overheating defects in which some parts or whole device may be damaged. Therefore, the coolers become an important part of many devices.

Coolers, based on its principle, can be divided into three groups: (1) passive coolers are based on the increase of surface area (using ribs, lamellas or rods) and are made from materials with high thermal

conductivity (as aluminium), (2) active coolers as fans are generating fluid flow from the environment, and (3) combined coolers, where the active cooler is deployed to the passive cooler and generates the flow of air passing through the passive cooler to increase the efficiency of waste heat removal. The character of the flow is of great importance also. The highest intensity of heat removal from the heat transfer surfaces is achieved when the flow could be considered as turbulent flow or impacts directly on cooled surfaces (so-called impact flow).

A very interesting example is the heat transfer (cooling) of the micro-electro-mechanical systems (MEMS) where the flow is often, due to small dimensions, laminar and therefore the heat transfer ratio is small. Example could be found in the numerical study of Timchenko et al. (2006) [1] where is performed numerical simulation of intensification of an electronic processor's cooling: the laminar airflow is heated from one-side and affected by the synthetic jet

Corresponding author: Petra Dancova, Ph.D., research areas: fluid mechanics, thermodynamics, heat transfer, boundary layers, experiments, synthetic jets. E-mail: petra.dancova@tul.cz.

from the other side. Laminar flow is disturbed by the synthetic jet (in work of Timchenko et al. (2005) the term “quasi-turbulent flow” is suggested [2]) and the transport phenomena increases. The study of Choi (2005) [3] shows how it is possible to improve processor cooling. Go and Mongia (2008) [4] investigated the hydrodynamics and thermal performance of the synthetic jets perpendicular to a confined duct bulk flow and flow across the heated surface as well. The thermal measurement was performed by a system of thermocouples. Investigation of the advanced dual piezoelectric cooling jets as microfluidic devices describes a paper of de Bock et al. (2012) [5]. Heat transfer was obtained from temperatures of a cooler, heater, inlet/outlet air, respectively, measured with the thermocouples.

Presented work is based on the research of a heat transfer on the heated plate affected by the impinging synthetic jet. A high level of turbulence intensity of the synthetic jet leads to a significant increase of the heat transfer intensity. Due to this advantage, there is a wide range of possible applications in the field of cooling highly thermally loaded parts in micro-electronics. More details about these applications can be found in, e.g., Trávníček et al. (2006 and 2010) [6, 7]. The task of impinging jets which are used for the heat/mass transfer has been studied intensively in recent years, e.g., Gillespie et al. (2006) or Arik (2007) [8, 9]. Nevertheless lot of works investigates heat transfer indirectly using naphthalene sublimation, for the summarizing study see the paper of Goldstein and Cho (1995) [10]. These types of experiments are based on the analogy between heat and mass transfer, where measured mass transfer data are transformed to the heat transfer with using the ratio, $Nu/Sh = (Pr/Sc)^n$ where Nu , Sh , Pr and Sc is Nusselt, Sherwood, Prandtl and Schmidt number, respectively. Exponent n can be found in the range of 0.33 to 0.42 in those equations.

This paper brings investigation of the heat transfer coefficient measured with thermoanemometry in a constant temperature mode. Motivation of this work

was a paper of Scholten and Murray (1996) [11] which describes convective heat transfer measurement with a hot film sensor and its correction considering the influence of shear stress.

2. Experimental Setup and Methods

Synthetic jet (SJ) is generated by the periodic motion of an actuator oscillating diaphragm. In this work, the SJ actuator is driven by two actuating loudspeakers (Monacor SP 60/4). The diameter of each loudspeaker diaphragm and the actuator emitting orifice is $D_D = 75$ mm, $D = 10$ mm, respectively. The SJ impacts on the aluminium plate (with dimensions of 350×260 mm²) in the distance H from the SJ emitting orifice (see Fig. 1 for the schematic view of the experimental arrangement). The SJ actuator is placed on a traverser, which enables setting of position in all directions, the heated plate is fixed. The heating foil (130×130 mm²) is firmly fixed on the plate bottom side. The foil is maintained on the constant temperature which is controlled with a system of the thermocouples connected to the PID regulator. The thermocouples are fastened in a part of the plate not influenced by the impact of the SJ.

The loudspeakers are working in phase and fed with the harmonic signal. A constant input power of 3 W is used during the experiments. The actuating working frequency, discussed in paragraph 4.1, is set as 74 Hz.

A DANTEC anemometer (90C10) in a constant temperature mode is used for measurement. A direct

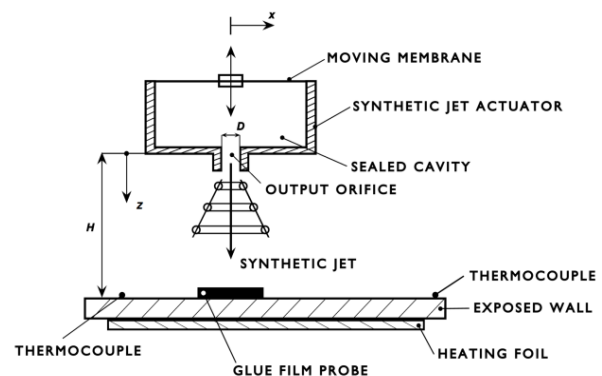


Fig. 1 Schematic view of the experimental setup.

single wire probe (55P11) is used for velocity measurements. The sampling frequency is 10 kHz and number of samples is 32,768. For the present experiments, the anemometer is calibrated in the range of (0.5-30.0) m/s. The error of the calibration due to the using of five-degree polynomial curve is less than 2%.

A glue-on film probe (DANTEC 55R47) fixed on the plate is used for heat transfer experiments. The sampling frequency and number of samples is also set as 10 kHz, 32,768, respectively. To minimize conductive losses from the probe to the plate, the probe should be adjusted to the same temperature as is set on the plate. The probe temperature is set by the overheat ratio a .

During the velocity and heat transfer experiments, the raw data of voltage are obtained. The phase averaging of these data during one cycle is performed by the decomposition $e(t) = \bar{E} + E_p + e'$, where \bar{E} , E_p , and e' (V) is the time-mean, periodic and fluctuating component, respectively. It should be taken into account that the thermoanemometric probes can measure only the absolute values of the flow. As the synthetic jet consists from the suction (negative values) and extrusion (positive values), it is necessary to determine the direction of the suction by data inverting during the data analysis. All data are processed using SW Matlab and Excel.

3. CFD Modelling

The CFD model is performed with respect to the experimental setup. The open source software OpenFOAM 4.0 with standard solvers is used for simulations. Transient numerical modelling consists of solving the pressure, velocity and thermal fields in a computational domain based on the momentum and energy with respect to the mass conservation. As assuming the incompressible turbulent flow, the transient solver *pimpleFoam* is chosen as a base for the development of a newly compiled solver for investigated problem. The *pimple* algorithm for solving momentum equation is used.

The simplified computational domain was defined based on the experimental setup. The computational domain has a cylindrical shape. Dimension H corresponds to the distance between the SJ output orifice and the exposed plate. The orifice output section is chamfered by the chamfer of size 1 mm x 45°.

The computational domain with $H = 50$ mm and a corresponding mesh were created by using the OpenFOAM tool *blockMesh*. Fig. 2 shows the schematic view of the domain (2a) and the computational mesh (2b).

Solver *pimpleFoam* does not contain method for solving of energy equation. So, it was necessary to modified original solver by adding an energy transport equation in the form [12]:

$$\frac{\partial T}{\partial t} + \nabla \cdot (\mathbf{U} T) - \nabla \cdot D_T \nabla T = 0 \quad (1)$$

where T (K) is thermodynamic temperature, t (s) time, and D_T (m^2/s) thermal diffusivity. Velocity vector \mathbf{U} (m/s) consists of three components U_x , U_y , U_z . The definitions of temperature fields and thermal diffusivity are implemented into the source code of the original solver. Newly compiled solver is named as *pimpleThermalFoam*. Air, considered as incompressible gas with constant density and viscosity, is used as a fluid in the whole computational domain. Turbulent model $k-\omega$ SST is used for modelling the turbulence and for the simulation of heat transfer in a boundary layer.

Defined boundary conditions are *inlet* and *heated wall* (see Fig. 2a). Unmarked faces are classified into one group named as *surroundings* which represents the interface between area of interest and ambient air in the laboratory. The inlet area represents the SJ actuator emitting orifice.

Velocity is defined by harmonic function, where the velocity value in z direction is defined as:

$$U_z = A \cdot \sin(2\pi f t) + B \quad (2)$$

where $A = 23.7$ m/s is the velocity amplitude, $B = 1.65$ m/s is the offset value, $f = 74$ Hz is the frequency and t (s) is time. Constants A and B are based on the

experimental data to reach good accordance with experimentally investigated velocity dependency on time. The sinusoidal curve CFD(in) in Fig. 3 represents the inlet velocity (defined by Eq. (2)). Other curves in Fig. 3 demonstrate following: EXP(or) illustrates experimental results measured at the point on the orifice axis in the distance 1 mm from the orifice output. CFD(or) shows the CFD results evaluated at the same point as is measured EXP(or).

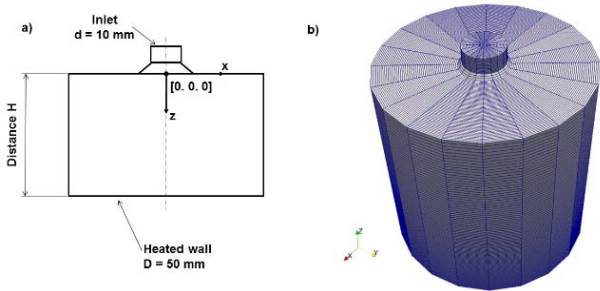


Fig. 2 Computational domain: a) geometry, b) mesh for $H = 50$ mm.

Table 1 Boundary conditions.

| Boundary | Pressure (Pa) | Velocity (m/s) | Temperature (K) |
|---------------------|-------------------------------------|---|--|
| <i>Inlet</i> | type zero Gradient | type uniform Fixed Value uniform Value sine (see Fig. 3) | type fixed Value value uniform 296.5 |
| <i>Heated wall</i> | type zero Gradient | type fixed Value value uniform (0 0 0) | type fixed Value value uniform 331 |
| <i>Surroundings</i> | type fixed Value value uniform 0 | type inlet Outlet | type fixed Value; value uniform 296.5 |

Main results from numerical simulations are velocity fields in the computational domain. The time parameter t/T is defined due to the transient solution and periodic changes at the inlet. Time parameters are set to evaluate results at $t/T = (0; 0.25; 0.5; \text{ and } 0.75)$, i.e., the beginning of suction, maximal suction, beginning and maximal extrusion, respectively.

4. Results and Discussion

4.1 Frequency Characteristics of SJ Actuator and Velocity Field Experiments

The SJ actuator works optimal near its resonance frequency, when it achieves the highest amplitude of the extrusion velocity; the mass flow rate of the fluid is maximal at the given power. Therefore, the frequency

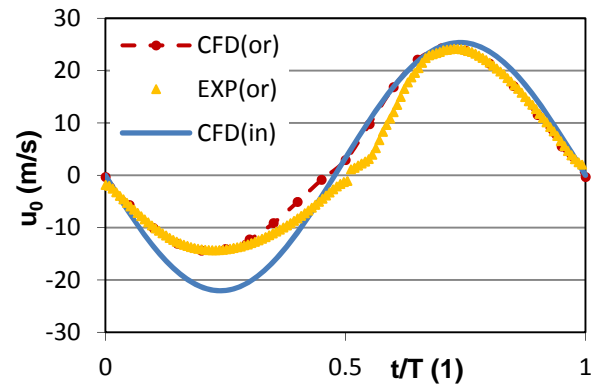


Fig. 3 Time varying velocity (CFD) compared with the experimental phased averaged velocity (EXP).

Heated plate is set as a wall with constant temperature on the surface. The temperature is the same as the maintained temperature in the experiments. Table 1 specifies the boundary conditions parameters important for the numerical model. Values which are not written in Table 1 are set with respect to the standard approaches in OpenFOAM [13].

characteristic of the SJ actuator has to be performed. Frequency determination is carried out by the thermoanemometry in a constant temperature mode using 55P11 probe. The probe was situated in the axis of the emitting orifice (z axis) at the distance $z/D = 1$. Resonance frequency is investigated for electric input power of the SJ actuator of 3 W and is found in the interval of (30-100) Hz. The error of the actuator electric power settings is within 0.6%. The maximum value of voltage/velocity is found at 74 Hz. At this frequency the velocity and heat transfer experiments are carried out. Fig. 4 shows the dependence of the dimensionless velocity on the frequency, where U_{res} means the velocity value obtained on the actuator resonance/working frequency. The value of the resonance frequency does not depend on the electric

power deviations during the power supply of the actuator, as visible in Fig. 4b.

To quantify the SJ parameters, the instantaneous velocity $u_0(t)$ is measured in the actuator orifice using CTA mode. Fig. 5 shows the velocity cycles for three different actuator input powers.

Summary of the SJ parameters is shown in Table 2. The time-mean orifice velocity U_0 and Reynolds

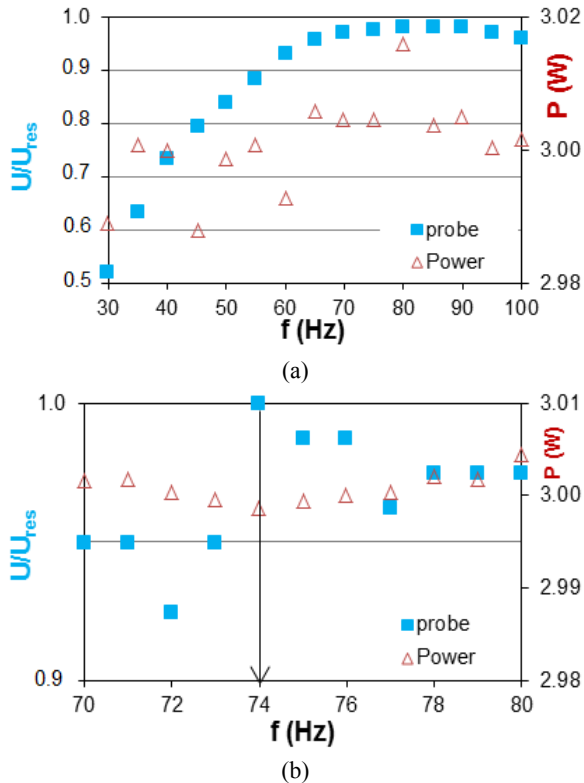


Fig. 4 (a) Frequency characteristic of the SJ actuator ($P = 3W$) (performed with a step of 5 Hz), (b) detailed view (step of 1 Hz). Filled squares and triangles represent velocity measured with the probe, and electric power supply of the SJ actuator, respectively.

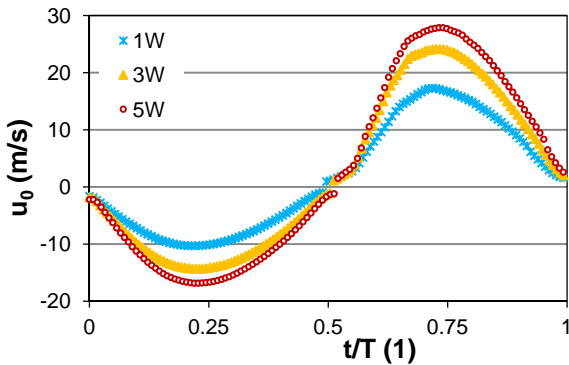


Fig. 5 Phased averaged velocity in the actuator orifice.

number Re_{SJ} of SJ used in Table 2 are defined by Eqs. (5) and (6):

$$U_0 = 1/T \int_0^{T_E} u_0(t) dt \quad (5)$$

$$Re_{SJ} = U_0 D / \nu \quad (6)$$

where T means the period of the cycle, i.e., $T = 1/f$ and f means the frequency, T_E means extrusion time ($T = T/2$ for the sinusoidal waveform as used in these experiments), $u_0(t)$ is the periodical axial orifice velocity. Another important parameter named *Extrusion stroke length* can be calculated as shows by Eq. (7):

$$L_0 = U_0 / f \quad (7)$$

Fig. 6 shows the development of the phase-averaged velocity U_p with increasing distance from the actuator orifice during one cycle of SJ actuator. The development of time-mean velocity U with increasing distance from the orifice is also presented. The velocity decreases with increasing distance in z direction and at the distance $z/D = 13$ from the orifice the flow oscillation practically disappears (the flow can be considered as a steady jet flow).

Table 2 Summarizing of SJ parameters.

| | 3 W |
|-------------|------|
| f (Hz) | 74 |
| U_0 (m/s) | 7.12 |
| L_0/D | 9.63 |
| Re_{SJ} | 4563 |

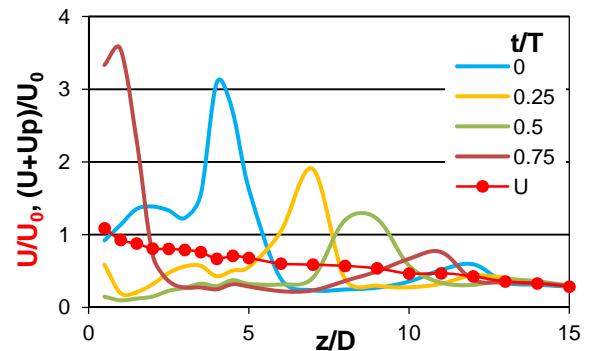


Fig. 6 Dependence of the phase-averaged velocity magnitude at different instances in the period and the time-mean velocity on the distance from the actuator orifice; $P = 3W$.

4.2 Heat Transfer Measurement

Experiments are performed with three overheat ratios $a = (0.07, 0.08, \text{ and } 0.12)$. Set values are listed see Table 3. The plate temperature should be set according to the Eq. (8) to prevent or minimize the conductive losses from the probe to the plate.

$$T_{\text{over}} + T_a \geq T_{\text{wall}} \quad (8)$$

Table 3 Temperature values settings.

| Overheat ratio a | Over temperature $T_{\text{over}} (\text{°C})$ | Ambient temperature $T_a (\text{°C})$ | Wire temperature $T_w (\text{°C})$ | Plate temperature $T_{\text{wall}} (\text{°C})$ |
|-----------------------|---|--|---------------------------------------|--|
| 0.07 | 20.83 | 23.5 | 44.33 | 43 |
| 0.08 | 23.81 | 23.5 | 47.31 | 46 |
| 0.12 | 35.71 | 23.5 | 59.21 | 58 |

Raw data, voltage, are processed with respect to the settings of the system resistance, i.e., total resistance, resistance of the probe wire and Wheatston's bridge resistance, respectively. Heat flux dissipated from the probe wire Q_{diss} (W) is then calculated in accordance with the paper of Scholten and Murray (1997) [14] as:

$$Q_{\text{diss}} = (E_{\text{SJ}}^2 - E_0^2) \frac{R_{\text{sensor}}}{(R_{\text{total}} + R_{\text{bridge}})^2} \quad (9)$$

where E_{SJ} and E_0 (V) means voltage through the probe wire measured if the SJ works, or the SJ is off (E_0). R_{total} , R_{sensor} , and R_{bridge} (Ω) are the whole system, probe, and Wheatston's bridge resistances respectively.

The dissipated heat transfer rate is calculated as:

$$q_{\text{diss}} = \frac{Q_{\text{diss}}}{1.5A_{\text{sensor}}} \quad (10)$$

where multiplication of the real probe wire area A_{sensor} with 1.5 gives the effective area of the sensor which is used to quantify lateral conduction within the film of the probe [15].

The Nusselt number is calculated as:

$$\text{Nu} = \frac{(q_{\text{diss}} + q_{\text{cond}})D}{k_{\text{air}}(T_w - T_a)} \quad (11)$$

where q_{cond} (W/m^2) is heat transfer rate through the probe film, D (m) diameter of the emitting orifice, and k_{air} ($\text{W}/(\text{m}\cdot\text{K})$) is mean value of thermal conductivity of

air in the boundary layer. The heat transfer coefficient is evaluated as:

$$h = \frac{q_{\text{diss}} + q_{\text{cond}}}{(T_w - T_a)} \quad (12)$$

where sum of over temperature, set through the overheat ratio a , and ambient temperature gives the value of the probe wire temperature. The wire and plate temperature difference is less than 1.33°C . The inequality " $>$ " is due to the PID regulator which sets the heating foil temperature (i.e., the temperature of the plate) within the control band.

Fig. 7 demonstrates dependence of the Nusselt number in the different instants of the period in different distances from the emitting orifice axis (axis z). The curves are shifted of 250 for clarify. Distribution of the phase-averaged and time-mean Nusselt number shows Fig. 8.

Fig. 9 brings the results of the time-mean values of the heat transfer coefficient measured in the distance $z/D = 5$. The measurement is made with three overheats ratios which corresponds to the over temperatures of 20.83°C , 23.81°C , and 35.71°C . The curves of h in Fig. 9 does not show as big difference of the dependence of h on the $(T_{\text{wall}} - T_a)$ which corresponds to the expected values. Fig. 10 shows the dependence of h on the phase of actuating period. As supposed, the highest heat transfer, the highest heat transfer coefficient respectively, occurs in the phase of maximal extrusion from the orifice ($t/T = 0.75$).

4.3 CFD Results

The results of CFD calculations are presented in form of velocity fields. According to the experiments, the velocity on the line which is coincident with the

orifice output axis is analysed. Velocity profiles are shown in Fig. 11.

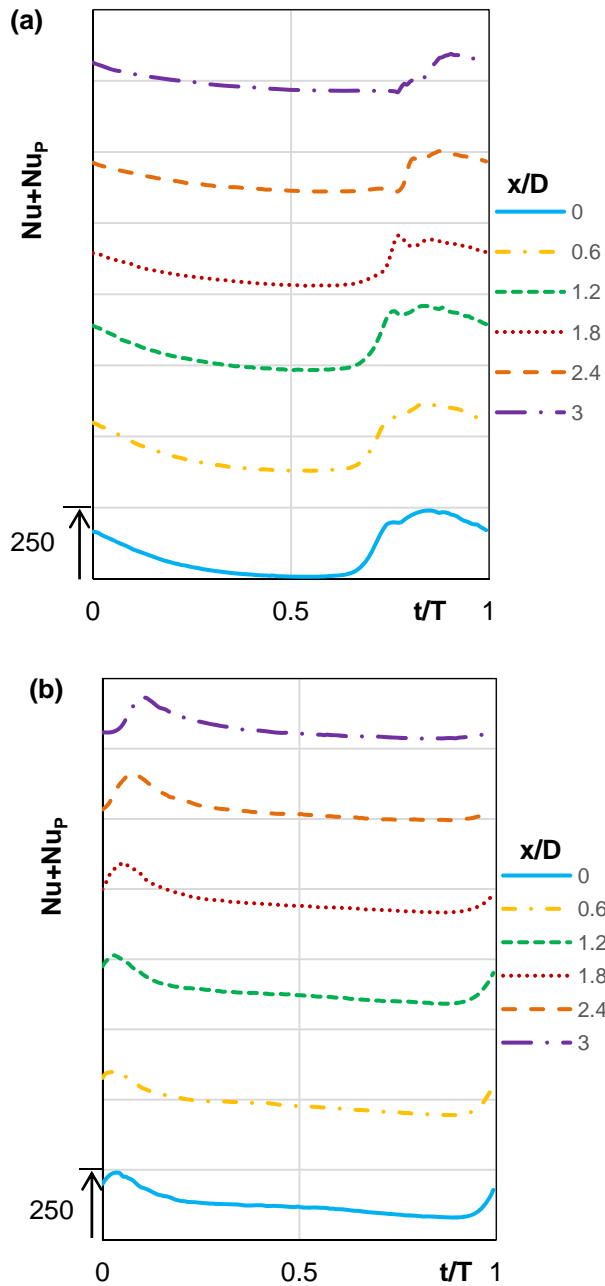


Fig. 7 Nusselt number dependence on the different instances in the period: (a) $z/D = 1$, (b) $z/D = 5$; $P = 3W$.

Comparison of the results obtained experimentally (shown in Fig. 6) with results from CFD (shown in Fig. 11) shows very good agreement of the phase averaged velocity magnitude profiles in the distance of z/D from 0 to 3. In the distance of z/D from 3 to 5 the velocity

profiles obtained from CFD are significantly affected by the presence of the wall. This effect is not consistent with the experimental results because that were measured in the free space (without the wall).

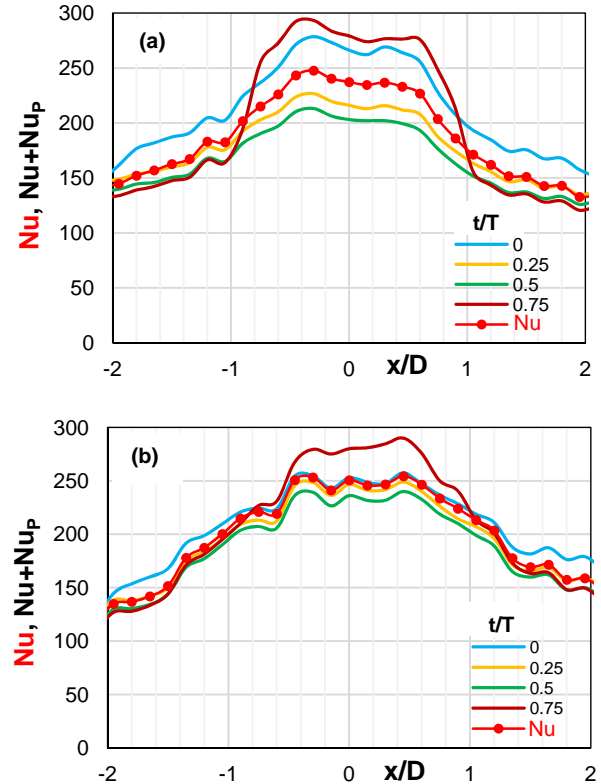


Fig. 8 Distribution of the phase-averaged ($Nu + Nu_p$) and time-mean Nusselt (Nu) number; (a) $z/D = 1$, (b) $z/D = 5$; $P = 3W$.

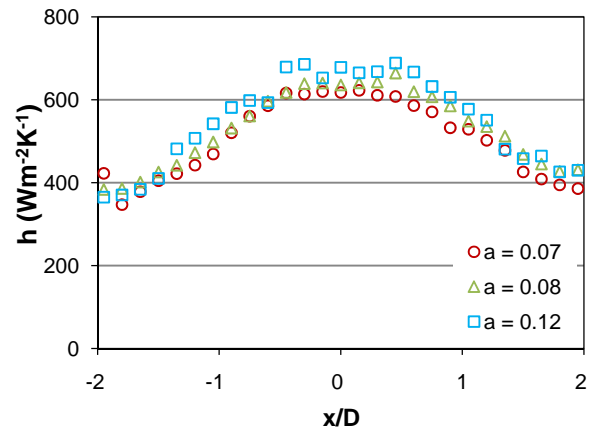


Fig. 9 Heat transfer coefficient (time-mean values) measured with set overhear temperatures of $20.83^{\circ}C$, $23.81^{\circ}C$, and $35.71^{\circ}C$; measured in distance $z/D = 5$; $P = 3W$.

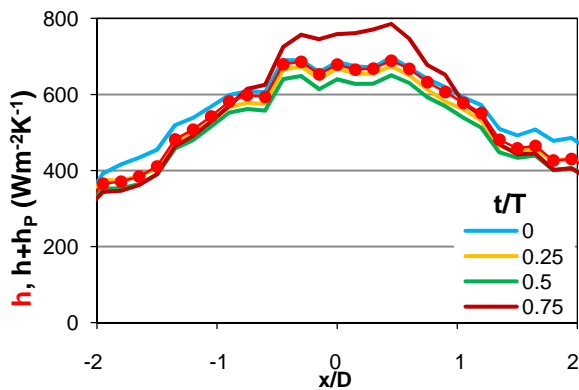


Fig. 10 Heat transfer coefficient (phased averaged) with overheating of 35.71°C ; measured in distance $z/D = 5$; $P = 3\text{W}$.

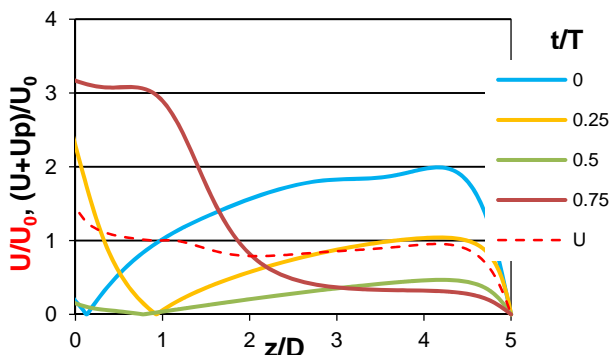


Fig. 11 Dependence of the phase-averaged velocity magnitude at different instances in the period and the time-mean velocity on the distance from the actuator orifice; CFD results.

5. Conclusions

This paper brings results of the synthetic jet experiments focused on the measurement of unsteady heat transfer coefficient by the glue-on thermoanemometry probe. As a first step, the working frequency of the SJ actuator was found as 74 Hz. On this frequency all experiments were carried out. From the velocity measurement, the time-mean orifice velocity U_0 and Reynolds number Re_{SJ} are determined as 7.12 m/s, and 4563, respectively. Heat transfer experiments were performed in the constant temperature mode of the thermoanemometer for three overheating ratios ($a = 0.07, 0.08, \text{ and } 0.12$), the over temperature was then set as 20.83°C , 23.81°C , and 35.71°C , respectively. According to the overheating ratios, the plate was heated to the temperature of (43, 46, and

58°C). Based on the thermoanemometer setting, i.e., setting of the whole system, probe and Wheatston's bridge resistances, the average and instantaneous values of Nusselt number and heat transfer coefficient were evaluated.

Experimental results of the SJ actuator working frequency and the velocity measured in the orifice output area were used for the development of the CFD solver based on the OpenFOAM platform. The experimental results of velocity profiles were used for the validation of the new-developed solver. After that the developed solver could be used with quite good accordance for solving the impinging synthetic jet. The first goal of the future work is to create a methodology to evaluate the heat transfer coefficient. The second one is the validation of the CFD solver to simulate heat transfer, especially in the near wall region. Then the experimental results shown in this paper will be used.

Acknowledgements

We gratefully acknowledge the support of the Grant Agency of the Czech Republic (Project No. 16-16596S) and the project SGS 21135 (Ministry of Education, Youth and Sports of the Czech Republic).

References

- [1] V. Timchenko, J. A. Reizes, E. Leonardi and F. Stella, Synthetic jet forced convection heat transfer enhancement in micro-channels, in: *Proceedings of the 13th International Heat Transfer Conference IHTC-13*, Sydney, NSW Australia, 2006.
- [2] V. Timchenko, J. A. Reizes and E. Leonardi, Heat transfer enhancement in micro-channels by synthetic jets, in: *Proceedings of the 4th International Conference on Computational Heat and Mass Transfer*, Paris-Cachan, France, 2005.
- [3] H. Choi, Active control of flows over bluff bodies for drag reduction, in: *Proceedings of the 6th Symposium on Smart Control of Turbulence*, Japan, 2005.
- [4] D. B. Go and R. K. Mongia, Experimental studies on synthetic jet cooling enhancement for portable platforms, in: *Proceedings of the 11th Intersociety Conference on Thermal and Thermomechanical Phenomena in Electronic Systems*, Orlando, FL, USA, 2008.
- [5] H. P. de Bock, P. Chamarthy, J. L. Jackson and B. Whalen, Investigation and application of an advanced dual

- piezoelectric cooling jet to a typical electronics cooling configuration, in: *13th IEEE IThERM Conference*, San Diego, CA, USA, 2012.
- [6] Z. Trávníček, T. Vít and V. Tesař, Hybrid synthetic jet as the non-zero-net-mass-flux jet, *Physics of Fluids* 18 (2006).
- [7] T. Trávníček, P. Dančová, J. Kordík, T. Vít and M. Pavelka, Heat and mass transfer caused by a laminar channel flow equipped with a synthetic jet array, *Journal of Thermal Science and Engineering Applications* 2 (2010) (4).
- [8] M. B. Gillespie, W. Z. Black, C. Rinehart and A. Glezer, Local convective heat transfer from a constant heat flux flat plate cooled by synthetic air jets, *Trans. ASME J. Heat Transfer* 128 (2006) 990-1000.
- [9] M. Arik, An investigation into feasibility of heat transfer and acoustic abatement of meso scale synthetic jets, *Appl. Therm.* 27 (2007) 1483-1494.
- [10] R. J. Goldstein and H. H. Cho, A review of mass transfer measurements using naphthalene sublimation, *Exp. Thermal and Fluid Science* 10 (1995) 416-434.
- [11] J. W. Scholten and D. B. Murray, Measurement of convective heat transfer using hot film sensors: Correction for sensors overheat, *Journal of Heat Transfer* 118 (1996) 982-984.
- [12] OpenFOAM, Foundation Course, Version 2.3.0 (2014)
- [13] OpenFOAM: User's guide, [online, cited 20.3.2018, available at:
<https://www.openfoam.com/documentation/user-guide/>
- [14] J. W. Scholten and D. B. Murray, Unsteady heat transfer and velocity of a cylinder in cross flow- I. Low freestream turbulence, *Int. J. Heat Mass Transfer* 41 (1997) 1139-1148.
- [15] D. E. Beasley and R. S. Figliola, A generalized analysis of a local heat flux probe, *J. Physics E.* 21 (1988) 316-322.